PUBLICATION 5

Modeling free convective mass and heat transfer in fuel cells

Submitted to Journal of Fuel Cell Science and Technology.

Modeling Free Convective Mass and Heat Transfer in Fuel Cells

Suvi Karvonen
VTT Technical Research Centre of Finland
Biologinkuja 5, Espoo, P.O.Box 1000, FI-02044 VTT, Finland
Tel. +358 40 136 7774
suvi.karvonen@vtt.fi

Abstract
The polymer electrolyte fuel cell (PEMFC) is a possible power source for many applications ranging from portable electronics to distributed energy production. In portable electronics the competition is mainly with batteries and the fuel cell system must be small and light. Using free-breathing fuel cells that take their oxygen from the surrounding air reduces the required volume of auxiliary equipment. However, managing the free convection induced mass and heat transfer is difficult and by necessity relies on passive methods and cell design. This work focuses on modeling heat and mass transfer on the cathode of a free-breathing fuel cell. A comparison of two- and three-dimensional models demonstrates that two-dimensional models do not give reliable results on the heat and mass transfer of such cells. The results also show that some earlier modeling efforts have been made using unnecessarily complicated or incorrect boundary conditions.

Nomenclature

Symbol	Quantity	Value/unit
c	concentration	mol/m^3
c_p	thermal capacity	J/kgK
D	binary diffusion coefficient	m^2/s
$\tilde{D}$	Maxwell-Stefan diffusion coefficient	m^2/s
E	energy	J
F	Faraday constant	96485 C/mol
$\mathbf{g}$	gravity vector	m/s^2
i	current density	A/ m^2
$\mathbf{j}$	molar flux vector	mol/m^2s
k	heat conductivity	J/m^2
M	molar mass	kg/mol
$\mathbf{n}$	normal vector	-
$\dot{\mathbf{N}}$	molar flux on electrode boundary	kg/m^2s
p	pressure	Pa
R	gas constant	8.314 J/molK
T	temperature	K
$\mathbf{t}$	tangential vector	-
q	thermal flux	W/m^2
$\mathbf{u}$	velocity vector	m/s
x	molar fraction	-
z	number of electrons involved in a reaction	-

Greek symbols

α	water transport number	-
ε	porosity	-
ρ	density	kg/m^3
κ	permeability	m^2
ω	mass fraction	-
η	dynamic viscosity	Pa s

1 Introduction

The polymer electrolyte membrane fuel cell (PEMFC) is a low temperature, small-scale fuel cell with a solid, proton conducting electrolyte membrane. PEM fuel cells could be used as a power source in portable electronics where they offer advantages over traditional batteries such as no need for recharging time and potentially more power density. However, before large-scale commercialization can take place, problems concerning the storage of the hydrogen fuel, reliability and life-time of the cell will have to be solved. The power density and efficiency of the fuel cell are also critical in terms of possible commercialization. In free-breathing fuel cells these attributes are strongly dependant on the effectiveness of the passive mass and heat transfer to ambient air.

A fuel cell system designed for use in portable electronics should be as compact as possible in order to minimize necessary auxiliary equipment. In a free-breathing fuel cell free convection in ambient air takes care of the heat and mass transfer on the cathode side of the cell. Free convection (a.k.a. natural convection) is caused by density variations in air resulting from temperature and concentration gradients generated by the operating fuel cell. Of these two, the temperature effect is usually more significant. The size, geometrical design and tilt angle of the fuel cell all affect the free convection phenomenon.

In this work, the mass and heat transfer driven by free convection was studied on the cathode to gain an understanding of how this effect should be modeled and how the different geometrical and operating parameters affect the heat and mass transfer. It should be noted that the model developed here is an example of a worst-case scenario in the sense that the ambient air is still and all movement is caused by natural convection, which is usually not the case. In reality, heat and mass transfer fluctuate according to wind or drafts and other disturbances as shown in e.g. [1].

The model consists of the cathode of a fuel cell and an ambient air zone surrounding the cathode. This corresponds to a fuel cell set in a larger portable application where the convection flow is blocked on one side by the device itself. Several simplifications were made in the modeling due to practical necessity. Only the cathode gas diffusion layer is included as a modeling domain and the cathode overpotential is taken as a constant across the active area. This is due to the fact that modeling the free convection in the ambient air requires a lot of computational capacity, and thus adding small-scale details such as the MEA would make the model computationally heavy. The product water of the cell reactions was assumed to be gaseous, i.e. two-phase flow conditions were not considered in this work. This decision was made partially due to necessity, since two-phase equations are complicated to solve, but mostly because of the fact that of the various required two-phase parameters, only a few have been properly either measured or theoretically derived. Most two-phase parameters derive from experiments made on sand or soil samples and using these values and correlations for a fibrous, partially hydrophobic material such as the GDL is questionable. However, should satisfactory values for the two-phase parameters be discovered, the results of this work apply also to making a two-phase model of a free-breathing fuel cell.

The aim of this work was to develop a good model of a free breathing fuel cell by comparing different approaches to modeling such cells. Here the focus is more on the free convection phenomenon and less on internal cell operation, thus complementing studies such as [2]. Different boundary conditions were studied to find the optimal one in 2D. Based on these results, a 3D model was built and its results were compared to those of the 2D models. This was done to evaluate whether 2D modeling of free-breathing fuel cells is reliable since it offers many advantages over 3D

models and has been used before, e.g. in [3]. The results show that some 3D models such as presented in [4] can be improved in terms of accuracy and computational efficiency by using different boundary conditions.

2 Theory

The models are divided into subdomains that include the ambient air zone, the cathode gas diffusion layer and the current collector ribs, the latter of which have to be excluded in the 2D model. The modeling domain is illustrated in Fig. 1. The area of the cell is 1 cm^2. The cathode catalyst layer is assumed to be an infinitely thin layer on the gas diffusion layer boundary. The size of the ambient air zone was chosen so that further increase in size no longer affected the results since if the zone is too small there is a risk of the natural convection mass transfer becoming more efficient than in reality.

The gas flow, species (nitrogen, oxygen and water) concentrations and temperature are modeled using the Navier-Stokes equations (in the ambient free convection zone), Darcy's Law (in the gas diffusion layer), continuity equation, Maxwell-Stefan diffusion and convection equation and the energy equation. The product water of the cell is assumed to be gaseous. This is typically not the case in a PEM fuel cell, but serves here as a first approximation. The authors are working on implementing a three-dimensional model that takes into account liquid water.

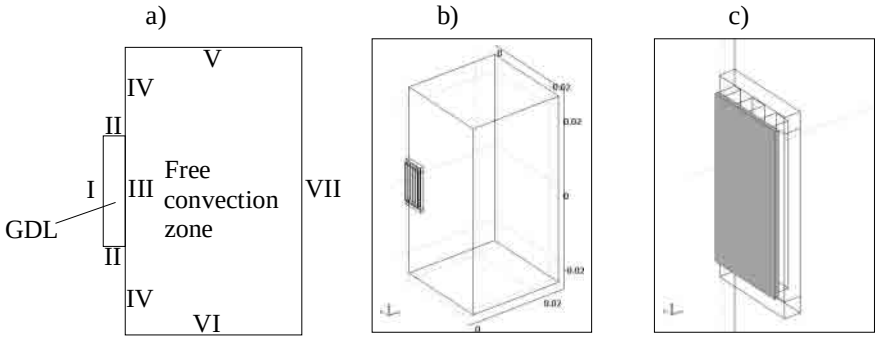

Figure 1. A schematic of the modeling domain in a) 2D (not in scale), b) 3D and c) the cathode GDL and current collector ribs enlarged in 3D. The shaded area in c) corresponds to the cathode GDL.

The equations used in the different modeling domains are standard electrochemical and mass transport equations used in fuel cell modeling with the effect of free convection derived buoyancy included.

Mass, momentum and energy transport:

$$-\rho\mathbf{u}\cdot\nabla\mathbf{u}+\rho\,\mathbf{g}-\nabla p+\nabla\cdot\left(\eta(\nabla\mathbf{u}+\nabla\mathbf{u}^{\mathrm{T}})\right)=0 \quad (1)$$

$$\nabla\cdot\left(\rho\frac{\eta}{\kappa}\nabla p\right)=0 \quad (2)$$

$$\nabla\cdot(\rho\,\mathbf{u})=0 \quad (3)$$

$$\nabla\cdot(k\nabla T)=c_p\rho\,\mathbf{u}\cdot\nabla T \quad (4)$$

The use of the Navier-Stokes equations (1) to model flow is acceptable with laminar flow (Reynolds number below 2000). For the Darcy equation (2), the Reynolds number has to be below 1. The first condition is satisfied in the whole modeling domain and the latter in the GDL. Consequently, Eq. (1) is used in the ambient air zone and Eq. (2) in the GDL. In the current collector ribs only energy transport is modeled.

Multicomponent diffusion equations (Maxwell-Stefan equations) were used to model diffusion in the model:

$$\nabla \cdot (\mathbf{j}_i + \rho \omega_i \mathbf{u}) = 0, \qquad i = \mathrm{O}_2, \mathrm{H}_2\mathrm{O}, \mathrm{N}_2 \tag{5}$$

$$\mathbf{j}_i = -\rho \omega_i \sum_{j=O_2,H_2O,N_2} \tilde{D}_{ij} \left(\nabla x_j\right), \tag{6}$$

$$\nabla x_j = \frac{M^2}{M_j} \sum_{\substack{j=O_2,H_2O,N_2 \\ k \neq j}} \left(\frac{1}{M} + \omega_k \left(\frac{1}{M_k} - \frac{1}{M_j} \right) \right) \nabla \omega_k \tag{7}$$

It should be noted that only two of the three (for oxygen, nitrogen and water) Maxwell-Stefan equations (5) have to be solved because the mass fraction of one species can be calculated from the other mass fractions since the sum of the mass fractions always has to equal one. Consequently, the mass fraction of nitrogen was calculated from those of oxygen and water, i.e. $\omega_{\mathrm{N}_2} = 1 - \omega_{\mathrm{O}_2} - \omega_{\mathrm{H}_2O}$. The Maxwell-Stefan diffusion coefficients $\tilde{D}_{ij}$ in the mass-averaged velocity frame are calculated from the binary diffusion coefficients D_{ij}, which were calculated with Equations (8) and (9) [5], as discussed in [6]. This calculation is equivalent with another formulation used in some articles, see e.g. [7].

$$D_{ij} = C \frac{T^{1.75} \sqrt{1/M_i + 1/M_j}}{p\left((v_i)^{1.3} + (v_j)^{1.3}\right)^2}, \text{ where } C \text{ is a constant (see Table (1)).} \tag{8}$$

The driving force for free convection is the density difference in air caused by temperature and composition differences. The temperature dependency of the density of air is calculated according to the ideal gas law:

$$\rho = -\frac{pM}{RT}, \qquad M = M_{\mathrm{N}_2} x_{\mathrm{N}_2} + M_{\mathrm{O}_2} x_{\mathrm{O}_2} + M_{\mathrm{H}_2O} x_{\mathrm{H}_2O} \tag{9}$$

Boundary Conditions

The boundaries of the 2D model are marked in Fig. 1 a). The 3D model has also thermally conductive current collectors. On the current collector boundaries, the temperature and its derivate are continuous and all the other fluxes are zero. The other boundaries are defined with appropriate boundary conditions listed in the following section.

Boundary I: the cathode catalyst layer. Oxygen is consumed and water and heat are generated on this boundary. Since the mass flux of generated water is not equal to the mass flux of consumed oxygen, there is total nonzero velocity across this boundary.

$$\rho \frac{\eta}{\kappa} \mathbf{n} \cdot \nabla p = (\dot{\mathbf{N}}_{O2} + \dot{\mathbf{N}}_{H2O}) / \varepsilon \rho \tag{10}$$

$$\mathbf{n} \cdot (\mathbf{j}_{H2O} + \rho \omega_{H2O} \mathbf{u}) = \dot{\mathbf{N}}_{H2O} \tag{11}$$

$$\mathbf{n}\cdot(\mathbf{j}_{O2}+\rho\omega_{O2}\mathbf{u})=\dot{\mathbf{N}}_{O2} \tag{12}$$

$$\mathbf{n}\cdot k\nabla T=c_p\rho\,\mathbf{u}\cdot\nabla T+q_0 \tag{13}$$

where $\dot{\mathbf{N}}_{O2}=\frac{i}{4F}M_{O2}$, $\dot{\mathbf{N}}_{H2O}=-\frac{i}{2F}M_{H2O}$ and $q_0=i\left(\eta+\frac{326T}{4F}\right)\cdot 0.8$ (the multiplier 0.8 follows from the assumption that 80 % of the generated heat is conducted out of the cell through the cathode side free convection).

The current density i on the catalyst layer boundary is calculated from the Butler-Volmer equation (14) and depends on the temperature and the mass fraction of oxygen on the catalyst boundary. The cathode overpotential is assumed constant. The water transfer coefficient α is 0.5.

$$i=i_0\frac{c_{O_2}}{c^0_{O_2}}\left(\exp\left(\frac{\alpha\, zF}{RT}\eta_c\right)-\exp\left(\frac{-(1-\alpha)zF}{RT}\eta_c\right)\right) \tag{14}$$

where i_0 is the temperature dependent cathode exchange current density calculated from [8]

$$i_0(T)=i_0(T_0)\exp\left(-\frac{\Delta E}{R}\left(\frac{1}{T}-\frac{1}{T_0}\right)\right) \tag{15}$$

where ΔE = 27 kJ/mol as discussed in [8].

Boundary II: Insulated GDL boundaries. There is no mass, heat or species transport across these boundaries.

$$\rho\frac{\eta}{\kappa}\mathbf{n}\cdot\nabla p=0 \tag{16}$$

$$\mathbf{n}\cdot(\mathbf{j}_i+\rho\omega_i\mathbf{u})=\mathbf{n}\cdot\mathbf{j}_i=0 \tag{17}$$

$$\mathbf{n}\cdot k\nabla T=c_p\rho\,\mathbf{u}\cdot\nabla T \tag{18}$$

Boundary III: Boundary between the GDL and the free convection zone. The momentum equation changes between Darcy's law and Navier-Stokes Equations. The effect of GDL porosity is taken into account as the difference (the multiplier ε) between the velocities in the gas diffusion layer and the free convection zone.

ω_{O_2}, ω_{H_2O}, and T are continuous across the boundary

$$\mathbf{u}_{Navier-Stokes}=\varepsilon\rho\frac{\eta}{\kappa}\mathbf{n}\cdot\nabla p_{Darcy} \tag{19}$$

$$p_{Navier-Stokes}=p_{Darcy} \tag{20}$$

Boundary IV: Insulated boundaries of the free convection zone.

$$\mathbf{u}=0 \tag{21}$$

$$\mathbf{n}\cdot(\mathbf{j}_i+\rho\omega_i\mathbf{u})=\mathbf{n}\cdot\mathbf{j}_i=0 \tag{22}$$

$$\mathbf{n}\cdot k\nabla T=c_p\rho\,\mathbf{u}\cdot\nabla T \tag{23}$$

Boundaries V, VI and VII: Free convection zone boundaries.

$$\mathbf{t}\cdot\mathbf{u}=0 \tag{24}$$

$$\mathbf{n}\cdot(\mathbf{j}_i+\rho\omega_i\mathbf{u})=\mathbf{n}\cdot\mathbf{u}\omega_i \text{ (Boundary V)} \tag{25}$$

$$\omega_{O_2}=\omega^0_{O_2},\ \omega_{H_2O}=\omega^0_{H_2O} \text{ (Boundaries VI and VII)} \tag{26}$$

$$T=T_0 \qquad \text{(Boundary VII)} \tag{27}$$

Alternative boundary conditions have also been used on these boundaries, see e.g. [8, 9]:

$$\mathbf{u} = 0 \tag{28}$$

$$\omega_{O_2} = \omega_{O_2}^0 \,,\ \omega_{H_2O} = \omega_{H_2O}^0 \text{ (Boundaries VI and VII)} \tag{29}$$

$$T = T_0 \qquad \text{(Boundary VII)} \tag{30}$$

In short, with the alternative boundary conditions the gas velocity is fixed to zero and temperature and mass fractions are fixed to those of ambient air on the outer boundaries of the free convection zone. Thus for the air flow the boundaries are "closed". The problem with this formulation is that a much larger modeling domain is required and the resulting free convection vortex can be problematic for the solver and typically more computing capacity is required since a finer mesh is necessary throughout the whole free convection zone. Both types of boundary conditions have been used in free convection modeling: for "open" boundaries, see e.g. [10] and for "closed" e.g. [9].

The governing equations (1-5) were solved with commercial finite element software, Comsol Multiphysics®. Depending on the cell dimensions, the models had 5000-10 000 elements, which corresponds to 60 000-120 000 degrees of freedom. The calculations were performed over a 64-bit client-server connection. The server computer had 12 Gb RAM and 40 Gb of swap-space. The operating system was SuSe 9.1 AMD64 Linux. The solution time with this hardware was from less than half an hour to a few hours.

3 Results

Quantities such as current density, temperature and mass fractions of water and oxygen were studied in the solved models. The aim was to find out how they vary between the 2D and 3D models and how changing the ambient air boundary conditions from open to closed affects these variables. This information allows for building a computationally efficient but still accurate model of a free-breathing fuel cell.

2D model and Boundary Conditions

Comparison of the results of 2D models with differently sized ambient air zones showed that the modeling domain has to be larger in the case of the closed boundary settings than with open, since otherwise the mass and heat transfer in the ambient zone will be overestimated. This causes the closed boundary settings to require more computing capacity. A sufficient distance for the boundaries from the fuel cell for both boundary settings was determined by enlarging the area until there was no significant difference resulting from further changes. The difference between the open and closed boundary conditions is shown in Fig. 2 and Fig. 3. The two flow fields are very different as a whole, but give similar results close to the cell.

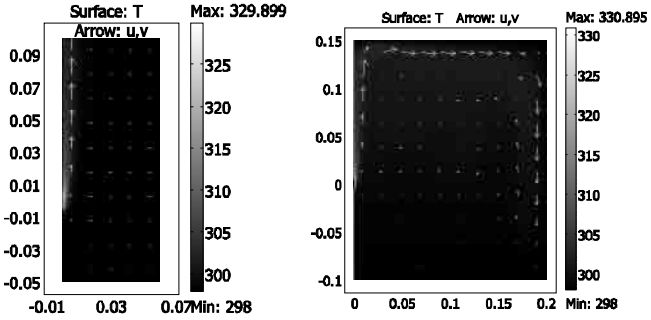

Figure 2. The flow fields and temperature distribution in the 2D models with a) open and b) closed boundary settings.

Comparison of the key parameters such as the current density and temperature of the cell show that with sufficiently large modeling domains, the differences between the two models are minute, less than 0.5 % for the current density and approximately 1 K for temperature. For the mass fractions, the differences are even smaller. In short, the closed boundary settings lead to slightly less efficient heat and mass transfer, presumably because the air velocity is a slower due to the zero-velocity boundaries. However, these differences are negligible. Thus both alternatives are suitable for modeling free convection. Using closed boundary conditions requires considerably more computing capacity and is thus impractical, especially for application in the 3D model. Based on these results the 3D model was implemented with the open boundary conditions.

3D model

The 2D model by necessity assumes a semi-infinite fuel cell with no cathode cover structures. The 3D model corresponds more accurately to reality since the width of the cell is limited and the current collector ribs are included. A similar model has been published in [2], however, the 2D modeling results of this work showed that the ambient air zone must large compared to the size of the cell and it is probable that this model overestimates the efficiency of natural convection.

As can be seen from results for current density, temperature and mass fractions illustrated in Fig. 3, there are significant differences between the two models. The current collector ribs affect the results in two ways: they hinder mass transfer as the gas flow cannot pass the solid ribs and improve the heat removal from the GDL. The latter is a consequence of the good thermal conductivity of the current collector which conducts the heat on to the current collector surface which is larger than the GDL surface and thus has better heat removal by natural convection.

The mass fractions on the catalyst layer do not differ much between the two models. The weaker mass transfer in the 3D model decreases the oxygen fraction and increases the water fraction in comparison to the 2D model. With oxygen, the change is negligible, in the order of 1 %, but with water vapor, the difference is above 10 %, which is large enough to strongly affect whether the cell is flooding or not. However, the most important differences are observed with the temperature and current density values. The ribs improve heat transfer and thus the temperature of the cell is 6 - 8 K lower in the 3D model. This is also reflected in current density according to Equations (12 and 13), which increases the current density for the 3D model. Thus a 2D model predicts higher temperatures and lower current densities than realistic since the ribs are excluded. It should also be noted that the lower temperature and higher water mass fraction in the 3D model both suggest that the 2D model can not be reliably used to predict flooding.

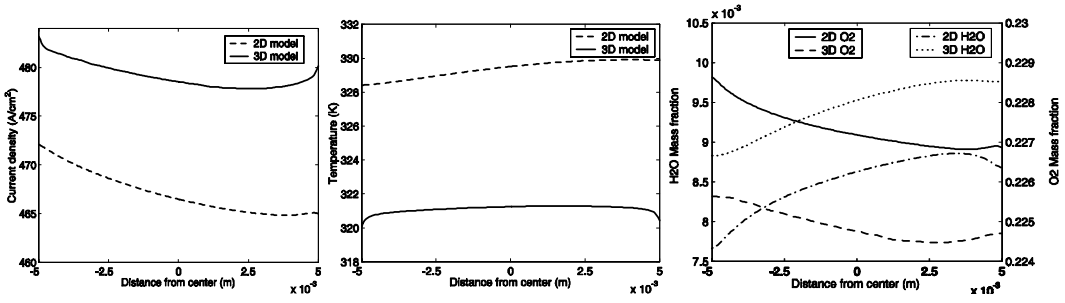

Figure 3. The a) current density, b) temperature, c) water and oxygen mass fractions on the catalyst layer. In the 2D model, the values are taken on the catalyst layer boundary and in the 3D model on the symmetry edge of the GDL catalyst layer surface (corresponding to a vertical middle line on the boundary). The left side corresponds to the bottom of the cell and the right side to the top.

The 3D model was also used for preliminary tests on the effect of cell size and tilt angle to the cell performance. Doubling the cell dimensions, i.e. quadrupling the area did not have a significant effect on the cell performance. This indicates that the cell size is small enough that free convection can provide sufficient reactants to the whole cell area.

4 Summary and Conclusions

Modeling is one approach to understanding the complex phenomena associated with free-breathing fuel cells. In this work, a model of a free-breathing fuel cell was developed in both two and three dimensions. The 2D model was used to optimize boundary settings and its results were used for building the 3D model. This model was used to study the natural convection phenomenon in the cathode of a free-breathing fuel cell and air surrounding the cell.

Comparing the results of the 2D and 3D models shows that 2D free-breathing fuel cell models can not, in general, be expected to give reliable data since heat and mass transfer efficiency is overestimated. This error is largely due to the fact that in 2D models the current collector ribs and any other support structures must be excluded and thus the 2D models give overly optimistic results for mass transfer while heat transfer is underestimated as the heat conduction through the ribs is absent.

Testing the boundary conditions with the 2D model showed that the two boundary condition settings gave similar results but one, the “closed” boundary conditions approach, required much more computing capacity. The similarity of the results suggested that both were applicable for modeling purposes, and thus the computationally less demanding “open” boundary settings were used in 3D modeling. It should be noted that other models of free-breathing fuel cells have typically used closed boundary settings, which makes them unnecessarily heavy.

The 3D model created in this work is computationally relatively light and can be used to study the effects of tilt angle, size and geometry to the cell performance. This is a subject for future work along with adding two-phase equations to the model.

References

[1] Tibor Fabian, Jonathan D. Posner, Ryan O'Hayre, Suk-Won Cha, John K. Eaton, Fritz B. Prinz and Juan G. Santiago: The role of ambient conditions on the performance of a planar, air-breathing hydrogen PEM fuel cell, J. Power Sources Volume 161, Issue 1 , (2006), Pages 168-182

[2] J. J. Hwang, W. R. Chang, C. H. Chao, F. B. Weng, and A. Su, Mass Transports in an Air-Breathing Cathode of a Proton Exchange Membrane Fuel Cell, J. Fuel Cell Sci. Technol. 6, 041003 (2009)

[3] S. Litster, J.G. Pharoah, G. McLeana and N. Djilali: Computational analysis of heat and mass transfer in micro-structured PEMFC cathode, Journal of Power Sources Volume 156, Issue 2, Pages 334-344 (2006)

[4] P. Manoj Kumar and Ajit Kumar Kolar**,** Effect of cathode design on the performance of an air-breathing PEM fuel cell, International Journal of Hydrogen Energy, Article in Press (2009)

[5] Taylor, Ross and Krishna, R.: Multicomponent Mass Transfer, John Wiley & Sons, Inc. (1993)

[6] C. F. Curtiss and R. Byron Bird: Multicomponent Diffusion, Ind. Eng. Chem. Res 38, 2525-2522, (1999)

[7] E. Birgersson, M. Noponen and M. Vynnycky: Analysis of a Two-Phase Non-Isothermal Model for a PEFC, J. Electrochem. Soc., Vol. 152, No. 5, pp. A1021–A1034 (2005).

[8] Wei Sun, Brant A. Peppley and Kunal Karana: An improved two-dimensional agglomerate cathode model to study the influence of catalyst layer structural parameters, Electrochimica Acta, Volume 50, Issues 16-17, Pages 3359-3374 (2005)

[9] S. Pretot, B. Zeghmati and G. Le Palec: Theoretical and experimental study of natural convection on a horizontal plate, Applied Thermal Engineering Volume 20, Issue 10, Pages 873-891 (2000)

[10] M. Havet and D. Blay: Natural convection over a non-isothermal vertical plate Int. J. Heat and Mass Transfer Volume 42, Issue 16, Pages 3103-3112 (1999)

Appendix

List of various constant and modeling parameters

Name	Symbol	Value
Dynamic viscosity	η	$1.81034 \cdot 10^{-5}$ Pa·s
Gravitational acceleration	g	9.81 m/s^2
Specific heat capacity of air	c_p	1005.38007 J/kg K
Ambient temperature	T_0	298 K
Universal gas constant	R	8.314 J/mol K
Ambient pressure	p_0	10^5 Pa
Heat conductivity of air	k	0.026044 J/m^2
Oxygen concentration in ambient air	$c_{O2,0}$	8.39128 mol/m^3
Water concentration in ambient air	c_{H2O0}	0.403621 mol/m^3
Faraday's constant	F	96485 C/mol
Molar mass of nitrogen	M_{N2}	0.0282 kg/mol
Molar mass of oxygen	M_{O2}	0.032 kg/mol
Molar mass of water	M_{H2O}	0.018 kg/mol
Effective heat conductivity of the GDL	k_{GDL}	0.3 W/m^2
GDL permeability	κ	$2.06 \cdot 10^{-12}$ m^2
Exchange current density	$i_0(T_0)$	0.01 A/m^2
Activation overpotential	η_c	0.6 V
GDL porosity	ep	0.5
Water transfer coefficient	α	0.5
Heat conductivity of the current collector	k_{cc}	14 J/m^2
Specific heat capacity of the current collector	c_{cc}	1000 J/kg K
Diffusion coefficient constant	C	$3.16 \cdot 10^{-8}$
Diffusion volume for oxygen	v_{O2}	$16.6 \cdot 10^{-6}$ m^3/mol
Diffusion volume for nitrogen	v_{N2}	$12.7 \cdot 10^{-6}$ m^3/mol
Diffusion volume for water	v_{H2O}	$17.9 \cdot 10^{-6}$ m^3/mol